Structural and vibrational properties of methane up to 71 GPa

Maxim Bykov,[1,2] Elena Bykova,[1] Chris J. Pickard,[3,4] Miguel Martinez-Canales,[5] Konstantin Glazyrin,[6]
Jesse S. Smith,[7] and Alexander F. Goncharov [1,*]

[1]*Earth and Planets Laboratory, Carnegie Institution of Washington, 5251 Broad Branch Road NW, Washington, DC 20015, USA*
[2]*Howard University, 2400 6th Street NW, Washington, DC 20059, USA*
[3]*Department of Materials Science & Metallurgy, University of Cambridge, 27 Charles Babbage Road, Cambridge CB3 0FS, United Kingdom*
[4]*Advanced Institute for Materials Research, Tohoku University, Aoba, Sendai 980-8577, Japan*
[5]*School of Physics and Astronomy and CSEC, University of Edinburgh, Peter Guthrie Tait Road, Edinburgh EH9 3FD, United Kingdom*
[6]*Deutsches Elektronen-Synchrotron DESY, Notkestr. 85, 22607 Hamburg, Germany*
[7]*HPCAT, X-ray Science Division, Argonne National Laboratory, Argonne, Illinois 60439, USA*

Single-crystal synchrotron x-ray diffraction, Raman spectroscopy, and first principles calculations have been used to identify the structure of the high-pressure (HP) phase of molecular methane above 20 GPa up to 71 GPa at room temperature. The structure of the HP phase is trigonal $R3$, which can be represented as a distortion of the cubic phase *B*, previously documented at 7–15 GPa and confirmed here. The positions of hydrogen atoms in the HP phase have been obtained from first principles calculations, which also demonstrated the stability of this structure above 260 K at 25 GPa. The molecules occupy four different crystallographic sites in phase *B* and 11 sites in the HP phase, which result in splitting of molecular stretching modes detected in Raman spectroscopy and assigned here based on a good agreement with the Raman spectra calculated from the first principles. Our study points out to a single HP phase unlike up to three HP phases proposed previously based on the Raman spectroscopy results only.

I. INTRODUCTION

Methane represents a rare and fundamental example of a hydrogen-bearing molecular compound with no hydrogen bonds unlike other simple molecules, HF, H_2O, H_2S, and NH_3. Thus, the crystal structure formation in methane solids is expected to be mainly determined by the steric effects and van der Waals bonds, suggesting that its behavior at high pressure may be similar to the rare gas solids, for example Ar [1], which persists in a face-centered-cubic (fcc) structure to very high pressures. Furthermore, the high-pressure behavior of methane is of interest to explore possible deviations from simple closed packed structures and related to this molecular orientational ordering, where the hydrogen atoms find the most energetically favorable stable positions. The fate of methane at even higher compression states in the regime of molecular proximity (i.e., shortened intermolecular H-H distances) is of great interest as it can be considered as a hydrogen dominant alloy [2] with the relevance to high-temperature superconductivity [3]. In addition, the behavior of methane at high pressures and temperatures may be of interest because it is believed to be a valued component of the deep planetary interiors of "icy" giant planets such as Uranus and Neptune [4]. Such hot molecular ices of water and ammonia form superionic crystals with diffusive protons at extreme pressure-temperature (*P-T*) conditions of relevance for these

planets [5–7], while methane tends to chemically react yielding oligomeric hydrocarbon compounds [8] and dissociate at higher *P-T* conditions yielding diamond and hydrogen [9–11].

Similar to Ar, methane crystallizes in phase I at about 1.5 GPa upon compression at room temperate forming a face-centered-cubic (fcc) closed packed structure of the molecular centers at the carbon atoms [12], and this crystal is plastic—molecules are freely rotating. However, unlike in noble gases, this structure transforms at 5.4 GPa to a complex rhombohedral structure *A* with 21 molecules in the unit cell solved by a combination of single crystal neutron and x-ray diffraction (XRD) techniques [13]. The structure is rhombohedrally distorted from the fcc methane I, with the carbon atoms occupying nine different crystallographic positions, and some of them may be associated with orientationally ordered molecules. However, the Raman and IR spectra do not show the obvious splitting of the major ν_1 and ν_3 C-H stretching modes [14].

Further compression leads to a transition to phase *B* with a very large unit cell containing 58 molecules, which has been found cubic as solved recently by Maynard-Casely *et al.* [15] for the carbon subsystem by combining powder and single-crystal XRD. The phase *B* shows a splitting of ν_1 and ν_3 stretching C-H modes in IR and Raman spectra [1,14,16,17], suggesting that it possesses some elements of orientational order (e.g., Refs. [14,16]). The transition from phase *A* to phase *B* at about 8 GPa is very sluggish and phase *B* can be missed if fast compressed yielding a simple cubic phase pre-*B* [16], where the Raman active ν_1 and ν_3 C-H stretching
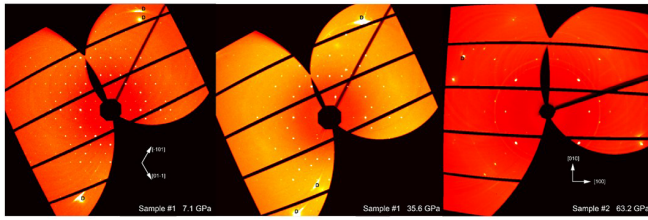
*agoncharov@carnegiescience.edu

FIG. 1. Reconstructed reciprocal lattice plane of methane visualized by CRYSALISPRO software package [24] at 7.07 GPa (left), 35.6 GPa (middle), and 63.2 GPa (right). D stands for diamond reflections. The observed diffraction spots from the sample have been indexed and used to determine the structure of phases *B* (left panel) and high-pressure (HP) phase (middle and right panels) (Table S1 and Tables I and II, respectively).

modes are not split, suggesting that methane molecules are orientationally disordered. Phase *B* is reported to transform to a high-pressure phase 1 (HP1) at about 25 GPa manifested by anomalies in IR spectra, vibrational frequencies [18], and specific volume [19], while no drastic structural changes were detected in the powder diffraction patterns. At higher pressures, Raman spectroscopy observations suggest further structural modifications to HP2 and HP3 phases reported up to 62 GPa [16]; however, the transition pressures to the subsequent high-pressure phases are contradictory [16,17]. The structure of the HP phase(s) has not been solved; it has been postulated to be cubic (e.g., Ref. [20]), but no detailed structural information is available. The XRD experiments have been extended to 202 GPa and the volume has been determined based on a cubic symmetry, even though a major transformation has been detected and a volume discontinuity was found at 94 GPa [20]. Methane was reported to persist in a molecular crystal structure beyond 200 GPa [20,21].

In this paper, we examine the structure of methane in the pressure range 7–71 GPa using single-crystal XRD, Raman spectroscopy, and first principles theoretical calculations. Our single-crystal XRD data directly determine the structure of the carbon subsystem in agreement with the previous report in phase *B* [15], while we find that the HP phase can be viewed as a rhombohedrally distorted phase *B* (space group *R*3) with 87 molecules in the unit cell (29 in the primitive unit cell); this structure remains unchanged between 20 and 73 GPa. We applied an *ab initio* random structure search of the most stable structures with and without any restriction of the symmetry. The results yield the structure of HP phase in agreement with XRD data, and determine the hydrogen positions in HP phase. The Raman spectrum of this phase calculated from the first principles is in a qualitative agreement with the experiment demonstrating that the C-H stretching mode splitting is due to a variation in the crystal field at different crystallographic sites.

II. EXPERIMENTAL AND THEORETICAL PROCEDURES

Methane gas was loaded in a mixture with He gas at approximately 1:1 mole ratio compressed to 0.15 GPa at room temperature in a BX90 diamond anvil cell [22] (Fig. S1 of the Supplemental Material [23]). In order to obtain good-quality single crystals of phase *B* of methane, the gas mixture was
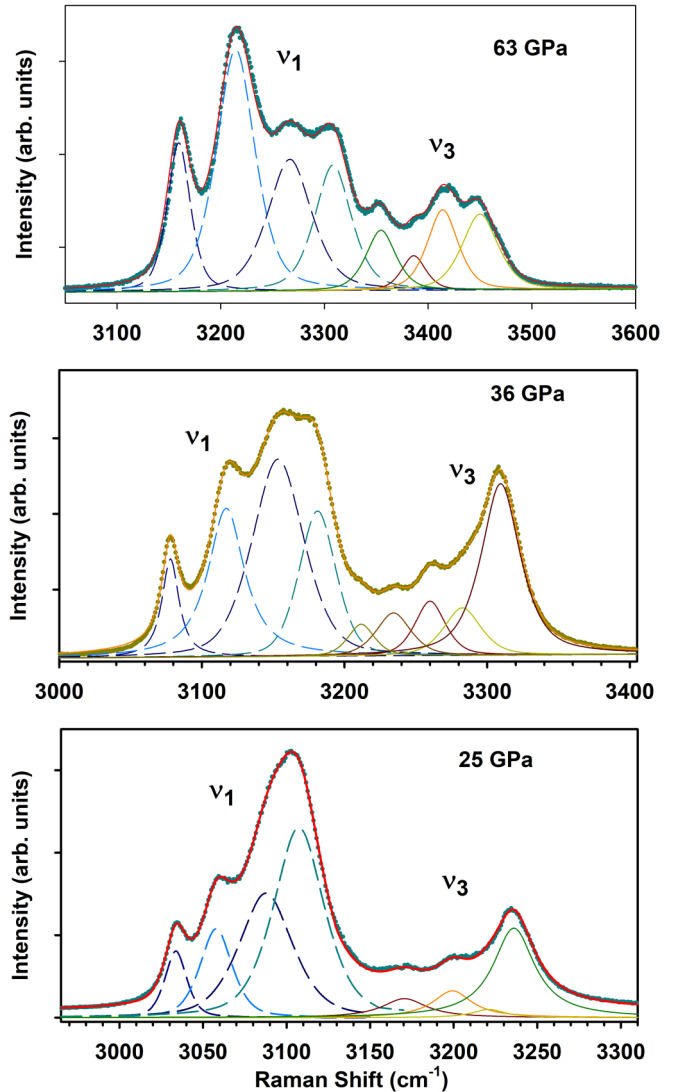

FIG. 2. Raman spectra of the C-H stretching modes of methane in HP phase at various pressures. The dots are the data and the lines are the fits to the Voigt oscillator model with eight (nine for the 36-GPa spectrum) peaks; variable color lines show the individual ν_1 (dashed) and ν_3 (solid) components. Note a change in the frequency scale in different panels due to a pressure shift.

slowly compressed at 297 K through the methane solidification point at 1.5 GPa and then to 8 GPa. At this pressure, excellent single crystals of phase *B* were grown overnight judging on Raman observations of a splitting of the ν_1 C-H

TABLE I. Comparison of agreement factors between *R*3 and *R*3*m* models of the HP methane.

| Pressure, GPa | No. of reflections | *R*3 model | | *R*3*m* model | |
		No. of parameters	R_1	No. of parameters	R_1
22.4	381	41	0.127	28	0.1303
27.4	474	41	0.138	28	0.1422
35.6	280	41	0.1020	28	0.1033
39.0	198	41	0.1415	28	0.1436

TABLE II. Crystal data, refinement and crystal structure details of Methane HP phase.

Pressure (GPa)	22.4	27.4	35.6	39.0
		Crystal data		
Crystal system, space group		trigonal, $R3$		
Z		87		
a, c (Å)	15.735(3), 9.660(2)	15.396(3), 9.481(2)	15.176 (8), 9.11 (7)	14.918(8), 9.14(7)
V (Å^3)	2071.3(7)	1946.1(7)	1818(13)	1762(14)
Radiation type		x ray, $\lambda = 0.344\,53$ Å		x ray, $\lambda = 0.2891$ Å
μ(mm^{-1})	0.02	0.02	0.02	0.02
		Data collection		
Diffractometer	GP @ ID16-B	GP @ ID16-B	GP @ ID16-B	GP @ P02.2
Absorption correction		Multi-scan		
No. of measured, independent and observed [$I > 3\sigma(I)$] reflections	676, 663, 381	640, 627, 474	475, 365, 280	792, 587, 198
R_{int}	0.111	0.026	0.039	0.059
$(\sin\theta/\lambda)_{\text{max}}$(Å^{-1})	0.752	0.768	0.586	0.664
		Refinement		
$R[F^2 > 2\sigma(F^2)]$, $wR(F^2)$, S	0.127, 0.136, 3.14	0.138, 0.150, 5.70	0.102, 0.117, 3.61	0.141, 0.149, 1.60
No. of reflections	663	627	365	587
$\Delta\rho_{\text{max}}, \Delta\rho_{\text{min}}$($e$Å^{-3})	0.32/−0.28	0.36, −0.37	0.25, −0.19	0.23, −0.20
		Crystal structure		
C1_1				
x	0	0	0	0
y	0	0	0	0
z	0.02(12)	0.02(8)	0.000(17)	0.013(9)
U$_{\text{iso}}$(Å^2)	0.09(11)	0.090(12)	0.049(8)	0.033(4)
C2_1				
x	0.0618(8)	0.0644(9)	0.0623(8)	0.0635(9)
y	0.1264(8)	0.1264(9)	0.1234(9)	0.1251(8)
z	0.33(12)	0.33(8)	0.340(16)	0.340(8)
U$_{\text{iso}}$(Å^2)	0.045(3)	0.035(3)	0.037(4)	0.050(3)
C2_2				
x	0.4816(9)	0.4801(9)	0.4844(8)	0.4863(8)
y	0.1468(9)	0.1451(9)	0.1485(8)	0.1476(7)
z	0.17(12)	0.17(8)	0.165(15)	0.174(8)
U$_{\text{iso}}$(Å^2)	0.041(3)	0.028(3)	0.028(3)	0.046(3)
C2_3				
x	0.6663(9)	0.6653(9)	0.6632(7)	0.6622(7)
y	0.1458(9)	0.1477(9)	0.1483(7)	0.1495(7)
z	0.17(12)	0.17(8)	0.162(16)	0.166(8)
U$_{\text{iso}}$(Å^2)	0.039(3)	0.028(3)	0.029(3)	0.041(3)
C2_4				
x	0.1216(7)	0.1230(8)	0.1256(7)	0.1245(7)
y	0.2456(7)	0.2449(8)	0.2489(6)	0.2506(7)
z	0.09(12)	0.09(8)	0.101(16)	0.093(9)
U$_{\text{iso}}$(Å^2)	0.041(3)	0.035(3)	0.034(3)	0.046(3)
C3_1				
x	0	0	0	0
y	0	0	0	0
z	0.67(12)	0.67(8)	0.666(16)	0.670(10)
U$_{\text{iso}}$(Å^2)	0.016(4)	0.014(4)	0.015(4)	0.049(6)
C3_2				
x	0.2388(6)	0.2376(7)	0.2361(6)	0.2339(7)
y	0.1208(6)	0.1174(7)	0.1178(6)	0.1175(7)

TABLE II. (*Continued.*)

Pressure (GPa)	22.4	27.4	35.6	39.0
z	0.14(12)	0.14(8)	0.152(15)	0.156(8)
$U_{iso}(Å^2)$	0.018(2)	0.014(2)	0.019(3)	0.039(3)
C4_1				
x	0.4644(8)	0.4595(8)	0.4648(7)	0.4635(7)
y	−0.0756(7)	−0.0774(8)	−0.0704(6)	−0.0730(7)
z	0.24(12)	0.24(8)	0.244(16)	0.239(8)
$U_{iso}(Å^2)$	0.047(3)	0.038(3)	0.036(3)	0.047(3)
C4_2				
x	0.0092(9)	0.0123(10)	0.0065(9)	0.0062(7)
y	0.3087(10)	0.3130(11)	0.3133(9)	0.3104(7)
z	0.33(12)	0.33(8)	0.339(16)	0.337(8)
$U_{iso}(Å^2)$	0.050(4)	0.049(4)	0.036(3)	0.038(3)
C4_3				
x	0.3005(8)	0.2991(10)	0.3080(9)	0.3070(7)
y	0.3121(9)	0.3081(11)	0.3116(9)	0.3122(7)
z	0.33(12)	0.33(8)	0.350(16)	0.342(8)
$U_{iso}(Å^2)$	0.047(4)	0.043(4)	0.037(3)	0.038(3)
C4_4				
x	0.2294(8)	0.2239(10)	0.2251(8)	0.2230(8)
y	0.4529(8)	0.4531(10)	0.4496(9)	0.4481(8)
z	0.19(12)	0.18(8)	0.166(15)	0.154(8)
$U_{iso}(Å^2)$	0.038(3)	0.039(3)	0.030(3)	0.040(3)

stretch mode (Fig. S2 of the Supplemental Material [23]). These crystals yield very sharp Bragg reflections with typical rocking-curve width of 0.64 ° at 7.1 GPa (Fig. 1). Two samples (nos. 1 and 2) were compressed up to 39 and 71 GPa respectively and concomitant XRD and Raman spectroscopy measurements (Figs. 1 and 2 and Fig. S2 of the Supplemental Material [23]) were taken at selected pressure points. All the experiments were performed at room temperature [295(2) K].

X-ray diffraction was performed at the beamlines 16-ID-B (APS, Argonne, USA) and P02.2 (Petra III, DESY, Hamburg, Germany). The following beamline setups were used. P02.2: $\lambda = 0.289\,Å$, beam size $\sim 2 \times 2\,\mu m^2$, Perkin Elmer XRD 1621 detector; 16-ID-B: $\lambda = 0.344\,Å$, beam size $\sim 3 \times 3\,\mu m^2$, Pilatus 1M detector. For the single-crystal XRD measurements samples were rotated around a vertical ω axis in a range $\pm 22°$. The diffraction images were collected with an angular step $\Delta\omega = 0.5°$ and an exposure time of 2–10 s/frame. For analysis of the single-crystal diffraction data (indexing, data integration, frame scaling and absorption correction) we used the crysalis^{pro} software package [24]. To calibrate an instrumental model in the crysalis^{pro} software, i.e., the sample-to-detector distance, detector's origin, offsets of goniometer angles, and rotation of both x-ray beam and the detector around the instrument axis, we used a
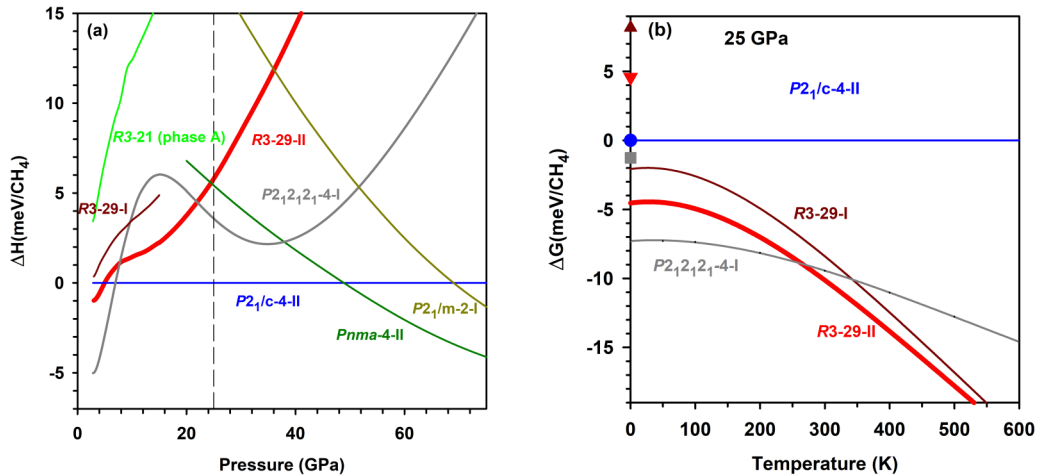

FIG. 3. (a) Theoretically calculated relative enthalpy of the most stable methane phases. The results for HP phase (*R3*-II) are shown by a thick red line. Other orientationally ordered phases are shown by thin lines of various colors. The vertical dashed line correspond to the pressure at which the temperature effects were taken into account. (b) Relative Gibbs free energies of the most stable methane phases as a function of temperature at 25 GPa. The symbols at $T = 0\,K$ represent relative classical enthalpies as computed with norm-conserving pseudopotentials.

TABLE III. Crystal structure of HP-CH_4 at 25 GPa optimized by calculations ($R3$, $a = 15.3315$, $c = 9.5221$ Å).

Site	x	y	z
C1_1	0	0	−0.9996
H1_1_1	−0.365 771	−0.622 456	−0.628 642
H1_1_2	0	0	−0.113 49
C2_1	−0.131 193	−0.066 507	−0.689 94
H2_1_1	−0.181 504	−0.146 561	−0.695 142
H2_1_2	−0.083 784	−0.042 373	−0.781 794
H2_1_3	−0.085 473	−0.048 146	−0.596 947
H2_1_4	−0.174 924	−0.029 387	−0.685 741
C2_2	0.148 245	0.474 857	−0.519 002
H2_2_1	0.079 276	0.476 659	−0.509 461
H2_2_2	0.205 456	0.534 268	−0.456 087
H2_2_3	0.136 305	0.402 921	−0.484 066
H2_2_4	−0.162 001	−0.181 677	−0.294 102
C2_3	−0.183 006	0.005 534	−0.191 981
H2_3_1	−0.255 161	−0.062 329	−0.199 231
H2_3_2	0.144 078	−0.273 369	−0.461 258
H2_3_3	−0.129 179	−0.010 913	−0.144 596
H2_3_4	−0.157 189	0.036 738	−0.295 11
C2_4	−0.252 732	−0.136 96	−0.448 695
H2_4_1	−0.285 273	−0.116 555	−0.534 236
H2_4_2	−0.300 828	−0.157 57	−0.357 472
H2_4_3	−0.243 439	−0.199 203	−0.480 598
H2_4_4	−0.180 176	−0.073 615	−0.422 955
C3_1	0	0	−0.346 612
H3_1_1	0.044 147	−0.032 218	−0.309 195
H3_1_2	0	0	−0.460 331
C3_2	−0.096 727	−0.545 671	−0.549 019
H3_2_1	0.173 063	0.094 993	−0.812 157
H3_2_2	−0.079 162	−0.473 773	−0.593 158
H3_2_3	−0.447 561	−0.266 257	−0.299 235
H3_2_4	0.299 905	0.127 484	−0.823 554
C4_1	−0.207 481	−0.422 449	−0.598 684
H4_1_1	−0.274 275	−0.422 628	−0.563 519
H4_1_2	−0.226 509	−0.496 916	−0.631 667
H4_1_3	−0.173 923	−0.371 07	−0.685 189
H4_1_4	−0.154 241	−0.399 094	−0.513 821
C4_2	−0.322 138	−0.356 324	−0.361 957
H4_2_1	−0.047 361	0.238 783	−0.656 792
H4_2_2	0.083 251	0.322 741	−0.659 402
H4_2_3	−0.334 52	−0.297 433	−0.322 463
H4_2_4	−0.323 976	−0.355 022	−0.475 03
C4_3	−0.316 752	−0.013 39	−0.682 065
H4_3_1	−0.308 246	0.013 518	−0.575 783
H4_3_2	0.281 839	0.313 491	−0.391 824
H4_3_3	−0.252 204	0.038 722	−0.743 068
H4_3_4	0.342 394	0.246 027	−0.349 393
C4_4	0.214 413	0.114 945	−0.509 708
H4_4_1	0.228 418	0.190 425	−0.496 222
H4_4_2	0.141 492	0.062 025	−0.467 591
H4_4_3	0.272 312	0.106 787	−0.457 289
H4_4_4	0.214 746	0.101 117	−0.620 706

single crystal of orthoenstatite [$(Mg_{1.93}Fe_{0.06})(Si_{1.93}, Al_{0.06})O_6$, *Pbca* space group, $a = 8.8117(2)$, $b = 5.18320(10)$, and $c = 18.2391(3)$ Å]. The same calibration crystal was used at both beamlines. The structure was solved with the SHELXT

structure solution program [25] using intrinsic phasing and refined with the JANA 2006 program [26]. Raman spectra were collected using the GSECARS Raman System [27] with the excitation wavelength of 532 nm and at the Earth and Planets Laboratory of Carnegie (EPL) using a 488-nm excitation line (e.g., Ref. [28]). Pressure was determined based on the shift of the $R1$ ruby fluorescence line [29].

Ab Initio Random Structures Searching (AIRSS) [30] was performed using the CASTEP code [31] to explore the structures of the HP methane with the rhombohedral symmetry (the unit cells with up to 87 atoms were explored), with a subsequent relaxation using density functional theory (DFT) calculations [31]. Raman spectra were computed using the density functional perturbation theory (DFPT) + finite differences method, using the default CASTEP 18 norm-conserving pseudopotentials with a 875-eV energy cutoff, and a k-point grid denser than $0.05 \times 2\pi/$Å.

III. RESULTS AND DISCUSSION

At pressures below ∼16 GPa, the diffraction pattern of CH_4 (Fig. 1) can be indexed with a body-centered-cubic unit cell of phase B (Table S1 and Fig. S3 [23]). Structure solution and refinement is in agreement with the model reported by Maynard-Casely *et al.* [15]. Due to weak scattering of hydrogen atoms, we were able to refine the positions of carbon atoms only. The unit cell contains four independent atomic sites: C1, C2, C3, and C4 occupying the positions $2a$, $24g$, $8c$, and $24g$, respectively. Therefore, there are 58 CH_4 molecules in the unit cell.

Further compression leads to a noticeable lattice distortion at above 18 GPa and the unit cell can no longer be considered cubic. This distortion is accompanied by the appearance of new modes in the Raman spectrum (Fig. 2 and Fig. S2 of the Supplemental Material [23]) in agreement with the previous observations [16,17] at similar pressure conditions. The most plausible indexing of the diffraction patterns of a methane high-pressure phase (HP) above 18 GPa can be performed using a rhombohedral unit cell (Tables I and II). Symmetry-lowering transitions from cubic I-$43m$ to rhombohedral symmetry may follow Γ_4 or Γ_5 irreducible representations with the following transformation of the lattice parameters:

$$\begin{pmatrix} \mathbf{a}_R \\ \mathbf{b}_R \\ \mathbf{c}_R \end{pmatrix} = \begin{pmatrix} -1 & 1 & 0 \\ 0 & -1 & 1 \\ 1/2 & 1/2 & 1/2 \end{pmatrix} \begin{pmatrix} \mathbf{a}_c \\ \mathbf{b}_c \\ \mathbf{c}_c \end{pmatrix},$$

where $\mathbf{a}_R$ $\mathbf{a}_R$, $\mathbf{b}_R$, $\mathbf{c}_R$ are lattice vectors of the rhombohedral unit cell (hexagonal setting), while $\mathbf{a}_c, \mathbf{b}_c, \mathbf{c}_c$ are lattice vectors of the cubic unit cell. The Γ_4 distortion leads to the space group symmetry $R3m$ (no. 160), while Γ_5 leads to $R3$ (no. 146). We should note that at pressures above 30 GPa we see a slight departure of the lattice parameters from R-centered hexagonal lattice ($a = b$, $\alpha = \beta = 90$, $\gamma = 120°$) suggesting a further monoclinic distortion. However, the degree of this distortion is not reproducible between two experiments (Fig. S4). Therefore, we conclude that this effect is related to the development of nonhydrostatic stresses in the sample, which is unavoidable at very high pressures and especially for very
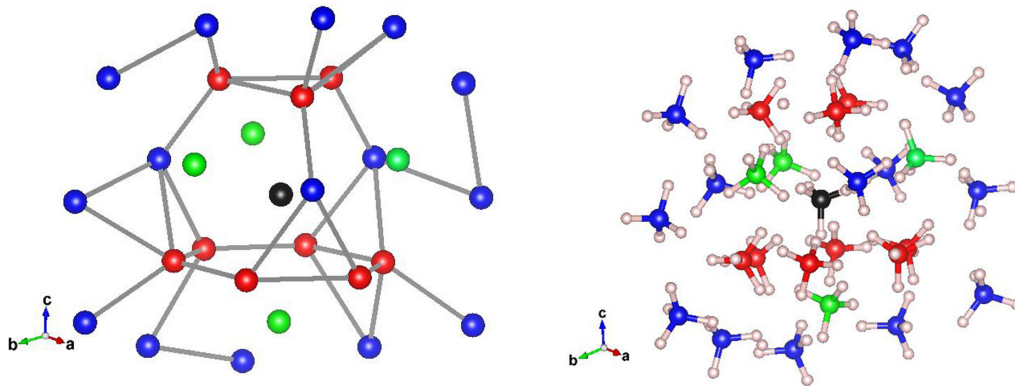
FIG. 4. Crystal structure of HP-CH$_4$ at 35 GPa. Black, red, green, and blue balls represent the positions of C1, C2, C3, and C4 carbon atoms, respectively; small pinkish circles are hydrogen atoms. Left panel shows C atoms only; gray lines connect the nearest C atoms with a cutoff of 3.08 Å.

soft crystals like methane. We therefore treat the high-pressure phase of methane as a single $R3$ phase.

We have tested both $R3$ and $R3m$ models (Table I). Although the $R3$ model has smaller agreement factors, they are not significantly different from those of the $R3m$ model. We have performed a Hamilton significance test in order to check if the improvement of the agreement factors for the $R3$ model may be considered significant [32]. For this test, both models were refined using the same set of reflections averaged based on the $R3$ symmetry. Based on the Hamilton test, the $R3$ model is preferable with the 75–90% confidence level depending on the pressure point. We, therefore, cannot completely reject the $R3m$ model based on the XRD data, but can conclude that the $R3$ model is more likely (Table I).

In order to complete the structure solution and determine the positions of hydrogen atoms, theoretical structure optimizations have been performed at various pressures (Fig. 3). First, we performed an *ab initio* random structure search (AIRSS) using the CASTEP code [31]. All calculations used the Perdew-Burke-Ernzerhof functional [33] together with the DFT-*D* dispersion correction scheme of Tkatchenko and Scheffler [34]. Among a plethora of phases marginally different in enthalpies, two structures emerged having $R3$ symmetries and 29 molecules in the primitive unit cell [$R3$-I and $R3$-II in Fig. 2(a)] in agreement with the experimental HP phase (Fig. 4). Both calculated $R3$ structures have equivalent carbon substructures and slightly different orientations of CH$_4$ molecules centered at the C4 atoms. According to the theoretical calculations both $R3$ structures are not the most energetically favorable at 0 K. However, if temperature effects are taken into account, the calculated Gibbs free energies show that the $R3$-II phase becomes the most favorable above 260 K at 25 GPa, which perfectly agrees with the experiment [Fig. 3(b)]. A monoclinic distortion noticed experimentally is found to be energetically unfavorable. Below we will mainly discuss the most energetically favorable $R3$ phase ($R3$-II, Table III).

The unit cell of HP-CH$_4$ (Fig. 4 and Fig. S5 of the Supplemental Material [23]) contains 11 symmetry independent carbon atoms with atoms C1_1 and C3_1 occupying positions $3a$, with the rest occupying positions $9b$. Here, the C atoms are named following the numbering for phase B [15] to show

the relation between B and HP phases, i.e., the atom C3_1 is generated from the atom C3 of the B phase.

Figure 4 shows the main motif of the most energetically favorable $R3$ structure. The C1_1 and C3_1 atoms that lie on the threefold axis possess a distorted tetrahedral icosi-octahedral environment. This polyhedron can be understood in the following way (see bottom of the Fig. S5 [23]): the atom C3_1 is coordinated by two six-membered rings, one of which is planar and capped, while the other is in a chair arrangement capped by a triangle. The packing of HP-CH$_4$ is primarily defined by intermolecular H-H interactions. The histogram of H-H distances has two distinct peaks (Fig. S6 [23]). The sharp peak at ∼1.75 Å corresponds to intramolecular H-H distances and almost does not shift with pressure as the molecules remain almost rigid under compression. The broad maxima at ∼2.05 and ∼1.95 Å at 20 and 30 GPa, respectively, correspond to closest intermolecular H...H contacts. These distances are in a good agreement with shortest intramolecular H...H contacts in compressed hydrogen [35].

The ν_1 and ν_3 C-H stretching Raman modes become composite (see also Refs. [16,17]) in phases B and HP suggesting either site symmetry or vibrational splitting. The Raman spectra collected at 25 GPa in the HP phase show that each of the ν_1 and ν_3 multifold can be well represented by four peaks (Figs. 2 and 5) except at 36 GPa, where an additional weak fifth peak tentatively assigned to the ν_3 fundamental is seen. On the other hand, theoretical calculations of the Raman activity of the HP phase performed in this work show a larger number of components, which correspond to various molecular sites as the analysis for the ν_1 modes shows (Fig. 5). However, the splitting pattern and value are qualitatively similar to the experimental; moreover, some theoretically calculated peaks are very close to each other making them difficult to resolve in the experiment; this likely results in broadened peaks, which consist of many components. A prominent feature of the ν_1 Raman spectra is a well split off low frequency peak that theory predicts is due internal vibrations of molecules involving C1 and C3 carbon in $3a$ sites, which are characterized by relatively more uniform in length and overall longer intermolecular distances (Fig. S7 [23]). This distinction results in a well-separated low-frequency ν_1 component, which can be also seen in
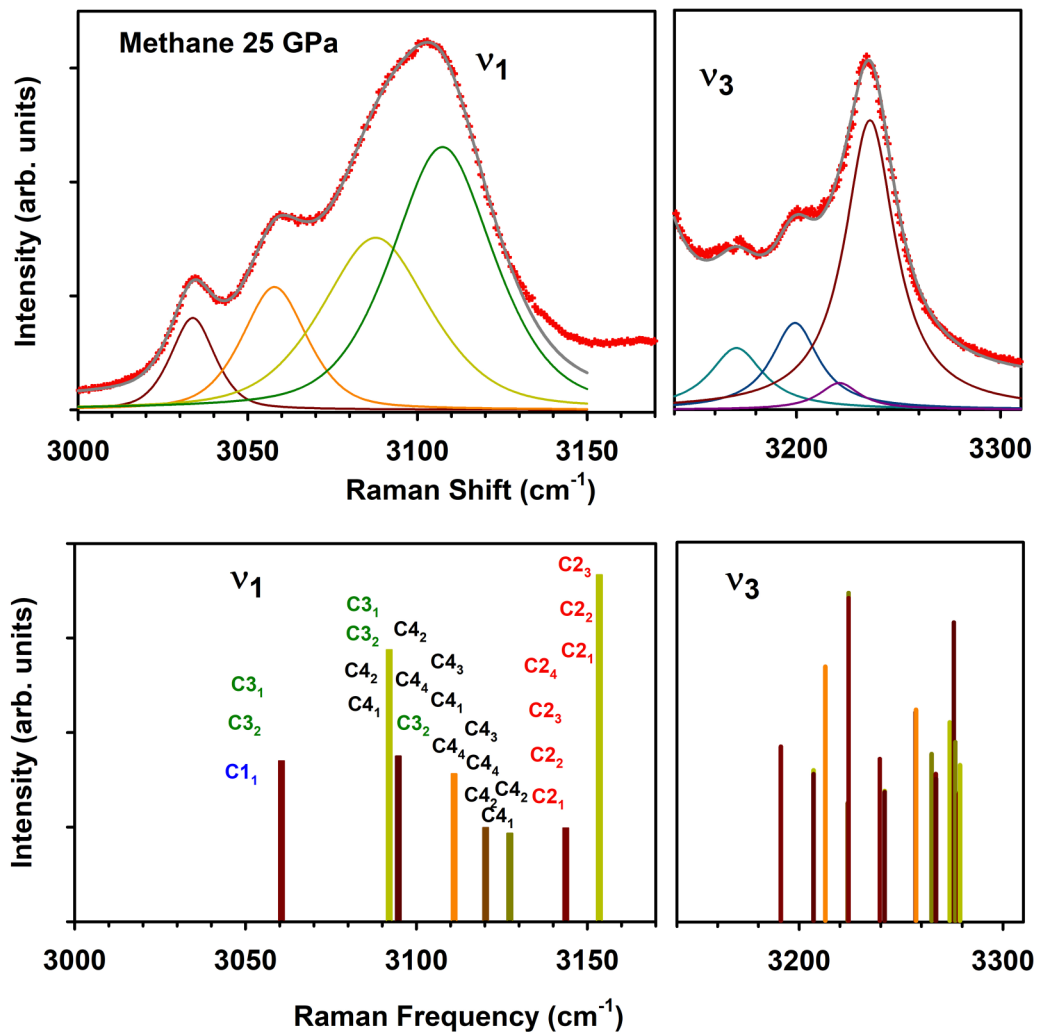
FIG. 5. Raman spectra of ν_1 (left panels) and ν_3 (right panels) stretching modes. The top panels are the spectrum measured at 25 GPa (488 nm excitation). Crosses are the data and gray line is the best fit to the Voigt oscillator model; variable color lines show the individual ν_1 and ν_3 components. The bottom panel shows the theoretically computed spectra at the same pressure. The labels (carbon atom sites) show the assignment of the peaks to the molecules of different kind. The experimental and theoretical peaks in the top and the bottom panels only slightly mismatch demonstrating a good correspondence of experiment and theory.

phase B with similar carbon site geometry save the lattice distortion.

The unit-cell parameters and symmetry of phases B and HP obtained here experimentally and theoretically provide reliable information on the P-V equation of state of methane (Fig. 6). Our results agree well with the previous determinations based on single-crystal [13,15] and powder [19,20,36] XRD. The cubic unit cell of phase B shows a distortion in the HP phase, which first appears small but then increases with pressure (Fig. S4 [23]). Please note that pre-B phase, which appears on fast compression of phase A, was indexed as a simple cubic lattice [19,20]; this phase is not examined with XRD here (but was detected by Raman spectroscopy to coexist with HP phase in the experiment no. 2 up to the highest pressure investigated) but it is clearly different from the HP phase of this study. HP and pre-B methane phases have very close volumes per the formula unit (Fig. 6) if one assumes that pre-B has 21 molecules in the unit cell as in phase A. Unlike previously reported modifications of

the HP phase based on changes in a number of ν_1 and ν_3 Raman components [16,17], our direct structural data (Fig. 1, Tables I and II) and analysis indicate that there exists only a single HP phase up to 71 GPa (cf. Refs. [16,17]), where the rhombohedral distortion gradually increases with pressure (Fig. S4 [23]). Consistently, we also find (by fitting the spectra using an oscillator models, Figs. 2 and 5) that the number of C-H Raman components remains essentially the same (cf. Refs. [16,17]) and their frequencies (Fig. 7) agree well with the results of previous Raman investigations [16,17]. The pressure dependencies of all the Raman frequencies can be approximated by sublinear curves (Fig. 7). Previous Raman investigations [16,17] reported minor changes in the spectra (peak splitting and changes in peak intensities) and in the P dependence of the C-H stretch frequencies. However, these changes do not signify the phase transitions, and, moreover, the inferred phase boundaries were inconsistent between these two investigations. The Raman peaks may split because they consist of a number of components, which have different
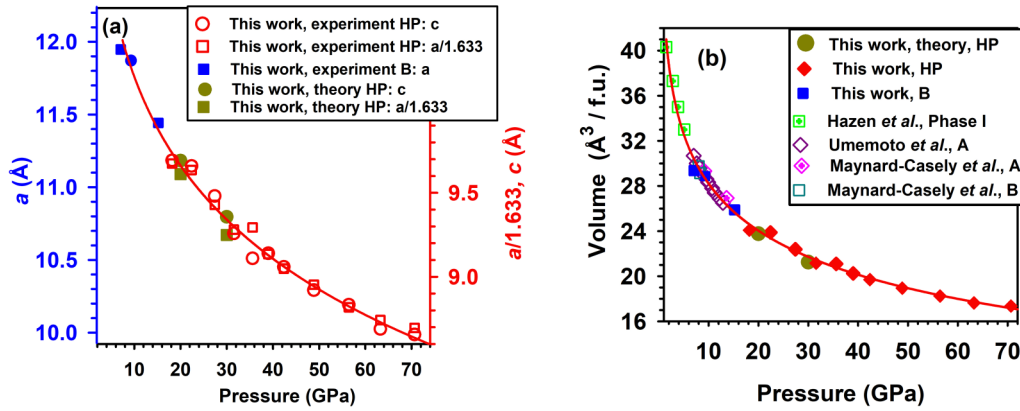
FIG. 6. Lattice parameters (a) and volumes per formula unit (b) of methane as a function of pressure. Note two vertical scales in the panel (a) for phases *B* (blue) and HP (red) which are scaled by a factor of $\sqrt{3}/2$ reflecting the difference in the unit cell dimensions. Also, the parameter **a** of the HP phase is divided by a factor of 1.633. Our experimental and theoretical volumes (b) are compared to previous experiments in phases I, *A*, *B*, pre-B, and HP [12,13,15,19,20]. The unit cell volume of pre-B methane of Ref. [20] was assumed to contain 21 formula units. The lines are guides to the eye.

pressure slopes so they become separated with pressure, while their relative intensity may change due to a number of reasons including the mode coupling and modification in the orientational order.

The unit cell volume changes smoothly through the *B*-HP transition suggesting a very small or no discontinuity. The theoretically computed lattice parameters and volumes are smaller than those determined theoretically, but the discrepancy is within 3%, which commonly is considered acceptable. However, this small difference may indicate that HP methane may still be partially disordered, which also corroborates with smaller (by some 20%) observed values of ν_1 and ν_3 multifolds splitting compared to the computed ones (Fig. 5). It is also worth noting that the measured and calculated Raman frequencies agree quite well, within 1.5%, demonstrating the validity of approximations made for computing the Raman spectra.

IV. CONCLUSIONS

Our concerted experimental and theoretical investigation determined the structure of the high-pressure HP phase of methane including the positions of hydrogen atoms. The structure is rhombohedral (space group $R3$) with 87 molecules in the unit cell. This extraordinary complex structure of approximately spherical molecules is in a drastic contrast with simple fcc (hcp) structures of noble gas solids. Moreover, the theoretically predicted orientationally ordered structures with smaller unit cell and with well elaborated intermolecular coupling schemes also do not capture the real structure. This indicates that the observed structure represents a balance between enthalpy and entropy terms thus suggesting that some molecular sites remain orientationally disordered; this makes this structure analogous to clathrates, where host and guest molecules are the same.

Our direct single-crystal XRD results suggest that there is only one high-pressure phase (HP) of methane between 20 and 71 GPa in contrast to previous works, which suggested up to three HP phases based on the results of Raman spectroscopy. The HP phase investigated here can coexist with a cubic pre-*B* phase investigated previously, the detailed structure of which still remains unknown.
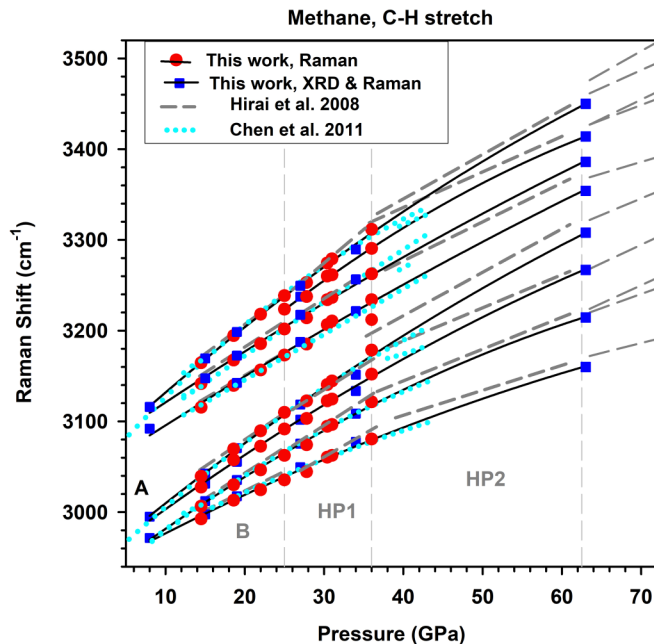

FIG. 7. Raman frequencies of the C-H stretching modes of methane as a function of pressure. Vertical dashed lines mark the phase transitions following Ref. [16]. The symbols are the results of two experiments of this work (solid line is the guide to the eye), while dashed and dotted lines represent the results of previously published works [16,17]. The data between 36 and 63 GPa could not be taken because the experiment to 63 GPa was performed at the x-ray synchrotron beamline, so the Raman spectra could only be measured at the last pressure point.

[1] P. Hebert, A. Polian, P. Loubeyre, and R. Le Toullec, Phys. Rev. B **36**, 9196 (1987).

[2] N. W. Ashcroft, Phys. Rev. Lett. **92**, 187002 (2004).

[3] E. Snider, N. Dasenbrock-Gammon, R. McBride, M. Debessai, H. Vindana, K. Vencatasamy, K. V. Lawler, A. Salamat, and R. P. Dias, Nature (London) **586**, 373 (2020).

[4] W. B. Hubbard, *Planetary Interiors* (Van Nostrand Reinhold, New York, 1984).

[5] C. Cavazzoni, G. L. Chiarotti, S. Scandolo, E. Tosatti, M. Bernasconi, and M. Parrinello, Science **283**, 44 (1999).

[6] S. Ninet, F. Datchi, and A. M. Saitta, Phys. Rev. Lett. **108**, 165702 (2012).

[7] V. B. Prakapenka, N. Holtgrewe, S. S. Lobanov, and A. F. Goncharov, Nat. Phys. (2021), doi: 10.1038/s41567-021-01351-8.

[8] S. S. Lobanov, P.-N. Chen, X.-J. Chen, C.-S. Zha, K. D. Litasov, H.-K. Mao, and A. F. Goncharov, Nat. Commun. **4**, 2446 (2013).

[9] F. Ancilotto, G. L. Chiarotti, S. Scandolo, and E. Tosatti, Science **275**, 1288 (1997).

[10] D. Kraus, J. Vorberger, A. Pak, N. J. Hartley, L. B. Fletcher, S. Frydrych, E. Galtier, E. J. Gamboa, D. O. Gericke, S. H. Glenzer, E. Granados, M. J. MacDonald, A. J. MacKinnon, E. E. McBride, I. Nam, P. Neumayer, M. Roth, A. M. Saunders, A. K. Schuster, P. Sun, T. van Driel, T. Döppner, and R. W. Falcone, Nat. Astron. **1**, 606 (2017).

[11] G. Gao, A. R. Oganov, Y. Ma, H. Wang, P. Li, Y. Li, T. Iitaka, and G. Zou, J. Chem. Phys. **133**, 144508 (2010).

[12] R. M. Hazen, H. K. Mao, L. W. Finger, and P. M. Bell, Appl. Phys. Lett. **37**, 288 (1980).

[13] H. E. Maynard-Casely, C. L. Bull, M. Guthrie, I. Loa, M. I. McMahon, E. Gregoryanz, R. J. Nelmes, and J. S. Loveday, J. Chem. Phys. **133**, 064504 (2010).

[14] R. Bini, L. Ulivi, H. J. Jodl, and P. R. Salvi, J. Chem. Phys. **103**, 1353 (1995).

[15] H. E. Maynard-Casely, L. F. Lundegaard, I. Loa, M. I. McMahon, E. Gregoryanz, R. J. Nelmes, and J. S. Loveday, J. Chem. Phys. **141**, 234313 (2014).

[16] H. Hirai, K. Konagai, T. Kawamura, Y. Yamamoto, and T. Yagi, Chem. Phys. Lett. **454**, 212 (2008).

[17] P.-N. Chen, C.-S. Zha, X.-J. Chen, J. Shu, R. J. Hemley, and H.-k. Mao, Phys. Rev. B **84**, 104110 (2011).

[18] R. Bini and G. Pratesi, Phys. Rev. B **55**, 14800 (1997).

[19] S. Umemoto, T. Yoshii, Y. Akahama, and H. Kawamura, J. Phys.: Condens. Matter **14**, 10675 (2002).

[20] L. Sun, W. Yi, L. Wang, J. Shu, S. Sinogeikin, Y. Meng, G. Shen, L. Bai, Y. Li, J. Liu, H. k. Mao, and W. L. Mao, Chem. Phys. Lett. **473**, 72 (2009).

[21] L. Sun, Z. Zhao, A. L. Ruoff, C.-S. Zha, and G. Stupian, J. Phys.: Condens. Matter **19**, 425206 (2007).

[22] I. Kantor, V. Prakapenka, A. Kantor, P. Dera, A. Kurnosov, S. Sinogeikin, N. Dubrovinskaia, and L. Dubrovinsky, Rev. Sci. Instrum. **83**, 125102 (2012).

[23] See Supplemental Material at http://link.aps.org/supplemental/10.1103/PhysRevB.104.184105 for methods, supplemental figures (S1–S5), and tables (S1–S5), and references [27–30,32,34].

[24] Rigaku Oxford Diffraction, *CrysAlisPro Software System, Version 1.171* (Rigaku Corporation, Oxford, UK, 2021).

[25] G. M. Sheldrick, Acta Crystallogr., Sect. A: Found. Adv. **71**, 3 (2015).

[26] V. Petricek, M. Dusek, and L. Palatinus, Z. Kristallogr. **229**, 345 (2014).

[27] N. Holtgrewe, E. Greenberg, C. Prescher, V. B. Prakapenka, and A. F. Goncharov, High Pressure Res. **39**, 457 (2019).

[28] A. F. Goncharov, P. Beck, V. V. Struzhkin, R. J. Hemley, and J. C. Crowhurst, J. Phys. Chem. Solids **69**, 2217 (2008).

[29] H. K. Mao, J. Xu, and P. M. Bell, J. Geophys. Res.: Solid Earth **91**, 4673 (1986).

[30] C. J. Pickard and R. J. Needs, J. Phys.: Condens. Matter **23**, 053201 (2011).

[31] S. J. Clark, M. D. Segall, C. J. Pickard, P. J. Hasnip, M. I. J. Probert, K. Refson, and M. C. Payne, Z. Kristallogr. - Cryst. Mater. **220**, 567 (2005).

[32] W. C. Hamilton, Acta Crystallogr. **18**, 502 (1965).

[33] J. P. Perdew, K. Burke, and M. Ernzerhof, Phys. Rev. Lett. **77**, 3865 (1996).

[34] A. Tkatchenko and M. Scheffler, Phys. Rev. Lett. **102**, 073005 (2009).

[35] V. Labet, P. Gonzalez-Morelos, R. Hoffmann, and N. W. Ashcroft, J. Chem. Phys. **136**, 074501 (2012).

[36] I. Nakahata, N. Matsui, Y. Akahama, and H. Kawamura, Chem. Phys. Lett. **302**, 359 (1999).